

УДК 539.1.074.4

HEAVY ION STUDIES WITH CMS HF CALORIMETER

*J.Damgov^a, V.Genchev^a, V.A.Kolosov^b, I.P.Lokhtin^c, S.V.Petrushanko^c,
L.I.Sarycheva^c, C.Yu.Teplov^c, S.V.Shmatov^d, P.I.Zarubin^d*

^aInstitute of Nuclear Research and Nuclear Energy, Sofia

^bInstitute of Theoretical and Experimental Physics, Moscow

^cM.V.Lomonosov Moscow State University,

D.V.Skobeltsyn Institute of Nuclear Physics, Moscow

^dJoint Institute of Nuclear Research, Dubna

The capability of the very forward (HF) calorimeter of the CMS detector at LHC to be applied to specific studies with heavy ion beams is discussed. The simulated responses of the HF calorimeter to nucleus-nucleus collisions are used for the analysis of different problems: reconstruction of the total energy flow in the forward rapidity region, accuracy of determination of the impact parameter of collision, study of fluctuations of the hadronic-to-electromagnetic energy ratio, fast inelastic event selection.

Рассмотрена возможность использования калориметра переднего направления (HF) установки CMS для исследований на пучках релятивистских ядер. На основе моделирования ядро-ядерных взаимодействий и сигнала («отклика») HF-калориметра был проанализирован ряд вопросов: реконструкция потоков полной энергии в области малых углов, точность определения прицельного параметра столкновений ядер, изучение флуктуаций отношения адронной компоненты полной энергии к электромагнитной, мониторинг интенсивности неупругих событий.

INTRODUCTION

The main goal of heavy ion programme at future CERN Large Hadron Collider (LHC) is the experimental study of the properties of strongly interacting matter at energy densities which are high enough for a relatively long-lived quark-gluon plasma (QGP) to be formed [1–3]. The ALICE [4] and CMS [5] projects will cover various aspects of heavy ion physics. Since CMS detector is optimized mainly for the search of the Higgs boson in proton-proton collisions via accurate measurements of the characteristics of high-energy muons, photons, electrons and hadronic jets, it can also be used for studying the so-called «hard probes» of the QGP in heavy ion collisions: heavy quarkonia suppression, jet quenching, high-mass dimuons [6, 7]. The challenge is to determine the behaviour of «colour dipole» (heavy quarkonium) or «colour charge» (hard quark or gluon) in dense QCD-matter due to medium-induced reinteractions. The maximal energy density and corresponding final state reinteraction intensity are expected to occur in central rapidity region, which is covered by the barrel ($|\eta| < 1.5$) and the end-cap ($1.5 \leq |\eta| \leq 3.0$) electromagnetic and hadronic calorimeters, as well as by the tracker and muon stations for rapidity of detected muon $|\eta| < 2.4$.

The CMS calorimetric system is complemented by quartz-fiber very forward (HF — «Hadron Forward») calorimeters in the rapidity region $3.0 \leq |\eta| \leq 5.0$, which can be interesting for heavy ion studies due to the following reasons:

1) For studying heavy quarkonium, hard jet and high-mass dimuon production processes in heavy ion collisions, it is extremely important to perform measurements for the events of different centrality (from peripheral to central collisions). It is expected that QGP might be produced in the most *central* heavy ion collisions at extremely high energy density up to $\varepsilon_0 \sim 0.5 \text{ TeV/fm}^3 \gg \varepsilon_{\text{crit}} \sim 1 \text{ GeV/fm}^3$ [8]. On the other hand, for studies of diffractive phenomena, properties of a coherent pomeron and collective nuclear effects [9] it is necessary to select *peripheral* events with a large collision impact parameter. Assuming that the collision impact parameter is measured, the experimentally observed effects can be compared with theoretical predictions for expected signals of a «new» physics [6]. Since very forward rapidity region in general is almost free of final state reinteractions, the (transverse) energy deposition in HF is determined mainly by initial nuclear geometry of a collision rather than by final state dynamical effects. It gives the advantage in determining the impact parameter of heavy ion collision via (transverse) energy deposition in HF calorimeter [10].

2) Moreover, due to insensitivity of very forward rapidity region to the details of nuclear collisions dynamics it can be used also for fast selection of inelastic nucleus-nucleus collisions basing on the strong correlation between energy flow in positive ($\eta > 0$) and negative ($\eta < 0$) calorimeter arms.

3) On the other hand, in some events very forward rapidity region can be a subject of studying new dynamical effects. In particular, the nonstatistical fluctuations of hadronic-to-electromagnetic energy ratio in very forward rapidity region observed in an event-by-event analysis, could be a manifestation of quark matter fireball formation in heavy ion collisions (Centrauro-like events) [11–13].

4) Finally, very forward rapidity region is the most energetic part of the spectrum as compared to barrel and end-cap regions. Thus the reconstruction of the total energy flow in HF calorimeter is important for testing energy hermetic construction of CMS calorimeter system.

The outline of the paper is as follows. The results of simulation of energy flow in very forward rapidity region obtained with HIJING model and estimation of a heavy ion collision parameter are discussed in Sect. 1. In Sect. 2 we consider the possibility for fast inelastic event selection and monitoring, using correlation between energy flow in positive ($\eta > 0$) and negative ($\eta < 0$) very forward rapidity directions. In Sect. 3 we give the short description of CMS HF calorimeter geometry and installation. In Sect. 4 we analyze the response of HF calorimeter to total energy flow in Pb–Pb collisions and influence of magnetic field. The accuracy of impact parameter determination via (transverse) energy deposition in HF calorimeter is discussed in Sect. 5. The response of HF calorimeter to the events with strong fluctuations of hadronic-to-electromagnetic energy deposition ratio is analyzed in Sect. 6.

1. ENERGY FLOW IN VERY FORWARD RAPIDITY REGION AND ESTIMATION OF A COLLISION IMPACT PARAMETER: HIJING PREDICTIONS

In this section we demonstrate the correlation between the impact parameter b of heavy-ion collision and total transverse energy flow E_T on the basis of the HIJING model [14] at the LHC energy scale. We also argue that the measurement of E_T produced in the forward rapidity direction allows one to avoid some possible uncertainties in the b determination, and estimate the accuracy of b measurement in the event-by-event analysis.

The multiplicity and transverse energy production in the nucleus-nucleus collisions in the ultrarelativistic energy domain is considered as a combination of hard processes with transverse momentum transfer $p_T \geq p_0$ and soft particle production. A transverse energy flow produced in hard processes described by perturbative QCD is associated mainly with minijet production, i.e., jets with $p_T \geq 2$ GeV [8].

The initial average transverse energy carried by (mini)jets in the rapidity intervals Δy is related to the collision impact parameter b by the formula [8]:

$$\langle E_T(b, \sqrt{s_{NN}}, p_0, \Delta y) \rangle = T_{AA}(b) \sigma_{\text{jet}}(\sqrt{s_{NN}}, p_0)_{\Delta y} \langle E_T^{\Delta y} \rangle, \quad (1)$$

where $\langle E_T^{\Delta y} \rangle$ is the average transverse energy per a (mini)jet in Δy interval, σ_{jet} is the cross section of (mini)jet production in corresponding nucleon-nucleon collision. The differential distribution $d\sigma/dE_T$ is:

$$\begin{aligned} \frac{d\sigma_{\text{jet}}}{dE_T}(\sqrt{s_{NN}}, p_0, \Delta y) &= \frac{1}{2} K \int_{p_0^2, \Delta y}^{s/4} dp_T^2 dy_1 dy_2 \sum_{i,j,k,l} x_1 f_i(x_1, p_T^2) x_2 f_j(x_2, p_T^2) \times \\ &\times \left[\frac{d\hat{\sigma}^{ij \rightarrow kl}}{d\hat{t}}(\hat{s}, \hat{t}, \hat{u}) + \frac{d\hat{\sigma}^{ij \rightarrow kl}}{d\hat{t}}(\hat{s}, \hat{u}, \hat{t}) \right] \frac{\delta(E_T - p_T)}{1 + \delta_{kl}}, \end{aligned} \quad (2)$$

where p_0 is the pQCD cut-off parameter, x_1 and x_2 are the fractional momenta of the initial partons i and j , and y_1 and y_2 are the rapidities of outgoing partons; $d\hat{\sigma}^{ij \rightarrow kl}/d\hat{t}$ expresses the differential cross section for a parton-parton scattering as a function of the kinematical Mandelstam variables \hat{s} , \hat{t} and \hat{u} ; $f_{i,j}$ are the structure functions. The summation runs over all parton species and the factor $K \sim 2$ is used to correct the lowest order pQCD rates for the effects of next-to-leading order terms. The value of $\sigma_{\text{jet}}(\sqrt{s_{NN}}, p_0)_{\Delta y} \langle E_T^{\Delta y} \rangle$ then is:

$$\begin{aligned} \sigma_{\text{jet}}(\sqrt{s_{NN}}, p_0)_{\Delta y} \langle E_T^{\Delta y} \rangle &= \frac{1}{2} K \int_{p_0^2, \Delta y}^{s/4} dp_T^2 dy_1 dy_2 \sum_{i,j,k,l} x_1 f_i(x_1, p_T^2) x_2 f_j(x_2, p_T^2) \times \\ &\times \left[\frac{d\hat{\sigma}^{ij \rightarrow kl}}{d\hat{t}}(\hat{s}, \hat{t}, \hat{u}) + \frac{d\hat{\sigma}^{ij \rightarrow kl}}{d\hat{t}}(\hat{s}, \hat{u}, \hat{t}) \right] \frac{p_t}{1 + \delta_{kl}}. \end{aligned} \quad (3)$$

Experimentally known effects of modification of quark and gluon structure functions by nuclear medium called parton shadowing [15] has not been included here. To take into account the shadowing effect we should modify the formula (3) by multiplying parton distributions by a corresponding correction term:

$$f_i(x_1, p_T^2) f_j(x_2, p_T^2) \longrightarrow R_i^A(x_1, p_T^2) f_i(x_1, p_T^2) R_j^A(x_2, p_T^2) f_j(x_2, p_T^2), \quad (4)$$

here the ratio $R_{i,j}^A \equiv f_{i,j/A}(x, p_T^2)/f_{i,j/N}(x, p_T^2)$, where $f_{i,j/N}(x, p_T^2)$ is the parton structure function for a free nucleon and $f_{i,j/A}(x, p_T^2)$ is the corresponding parton distribution in a proton inside the nucleus.

The nuclear density overlap function of two colliding nuclei at a given impact parameter $T_{AA}(b)$ is calculated in the assumption of the Wood–Saxon nuclear density distribution $\rho_A(r)$:

$$T_{AA}(|\mathbf{b}|) = \int d^2\mathbf{r} T_A(\mathbf{r}) T_A(\mathbf{b} - \mathbf{r}), \quad (5)$$

where \mathbf{r} is a 2-dimensional vector defining the interaction point. The nuclear thickness function

$$T_A(|\mathbf{r}|) = \int dz \rho_A(\sqrt{|\mathbf{r}|^2 + z^2}). \quad (6)$$

The expression (1) relating E_T and b includes a term arisen from (semi)hard processes with $p_T \geq 2$ GeV only. For a more correct estimation of the collision impact parameter we should take into account, in addition, the part of a total transverse energy flow produced in soft interactions

$$\begin{aligned} \langle E_T \rangle^{\text{total}} &= \langle E_T \rangle^{\text{jet}} + \langle E_T \rangle^{\text{soft}}, \\ \langle E_T \rangle^{\text{soft}} &= T_{AA}(b) \sigma_{\text{soft}} \langle E_T^{\Delta y} \rangle^{\text{soft}}, \end{aligned} \quad (7)$$

where $\langle E_T^{\Delta y} \rangle^{\text{soft}}$ is the averaged transverse energy per particle produced by soft interactions. But soft processes cannot be calculated by pQCD applications, and phenomenological models [16, 17] should be used for the estimation of a soft part of the total energy flow.

As we already discussed in Introduction, main signatures of a possible QGP production are expected in the midrapidity region. One of the discussed features of such a state of nuclear matter is energy loss of scattered partons due to medium-induced final state interactions called jet quenching (see reviews [18, 19] and references therein). Among other effects originated by jet quenching one may expect a significant modification in the distributions of the transverse energy flow and charged multiplicity, $dE_T/d\eta$, $dE_T^\gamma/d\eta$, and $dn_{\text{ch}}/d\eta$ [10].

Indeed, an indication is found for ultrarelativistic energy domain concerning the appearance of a wide bump in the interval $-2 \leq \eta \leq 2$ over a pseudorapidity plateau of such distributions due to jet quenching. Figure 1 demonstrates the evolution of the effect with collision impact parameter variation (HIJING prediction). Since jet quenching due to final state reinteractions is effective only for the midrapidity region (where the initial energy density of minijet plasma is high enough), very forward rapidity region, $3 \leq |\eta| \leq 5$, remains practically unchanged. Therefore the large η region can be used for the collision impact parameter estimation with minimal dependence on possible signals of new physics in the central rapidity region.

The total cross section of AA collisions is calculated in the framework of a HIJING hybrid model of nucleus-nucleus interactions [14], where the cross section of hard processes is defined by the formula (3). The contribution of the soft low- p_t part of a produced particle spectrum has been simulated by using the FRITIOF and DPM models [16, 17]. In these models hadrons are considered as relativistic strings excited at hadron interactions. Calculations show that for central Pb–Pb collisions at the LHC energy the inclusive cross section of soft interactions at nucleon-nucleon collisions at corresponding c.m.s. energy is equal to 57 mb, while the inclusive cross section of hard processes is equal to 54 mb. The parton shadowing effect has been taken into account with default HIJING sets.

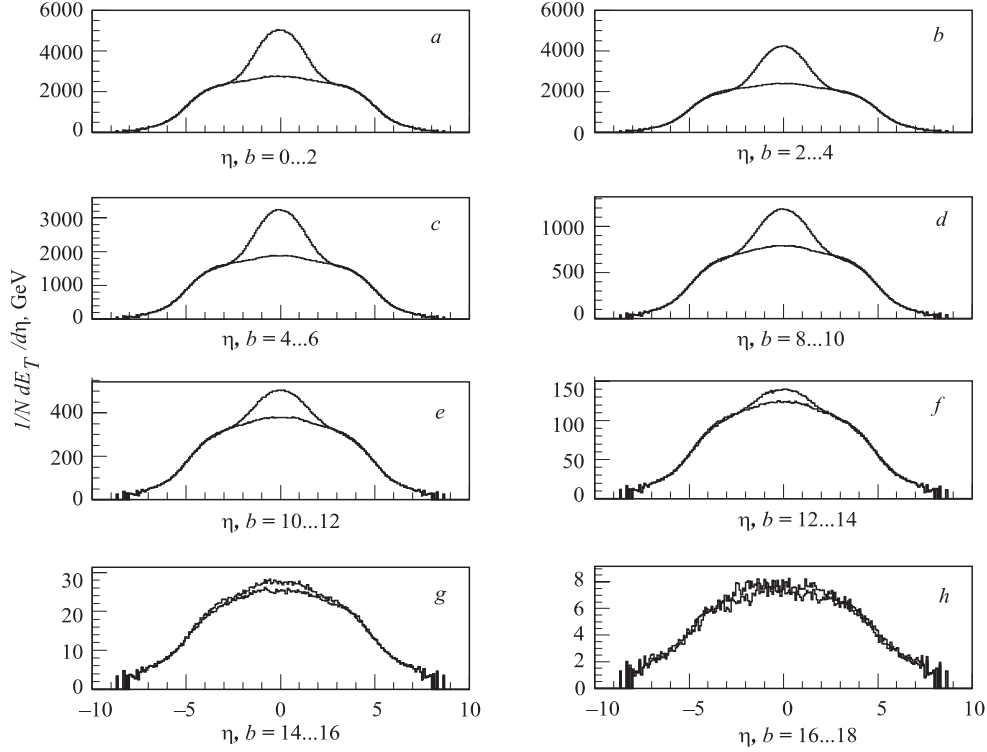


Fig. 1. Normalized differential distribution of the total transverse energy $dE_T/d\eta$ over pseudorapidity η for 10,000 minimum bias Pb–Pb collisions at $\sqrt{s} = 5.5A$ TeV for various impact parameters. The two cases are included: with jet quenching (the top line) and without jet quenching (the lower line)

Note that the average transverse energy of partons produced in hard processes $\langle E_T \rangle^{\text{jet}}$ (3–5 GeV for $|\eta| \leq 0.5$) is larger than the average transverse energy of soft partons $\langle E_T \rangle^{\text{soft}} \sim 0.4$ GeV. This fact reduces more strongly the relative contribution of soft processes in the total transverse energy production. In the LHC energy domain the hard and semihard processes contribute over 80% to the transverse energy in heavy ion collisions [8]. This allows one to reduce ambiguities of E_T calculations induced by the use of phenomenology models taking into account low- p_T processes.

In the framework of the HIJING model we have simulated 10,000 events of minimum bias Pb–Pb, Nb–Nb, Ca–Ca interactions at c.m.s. energy 5.5 TeV per nucleon pair. The

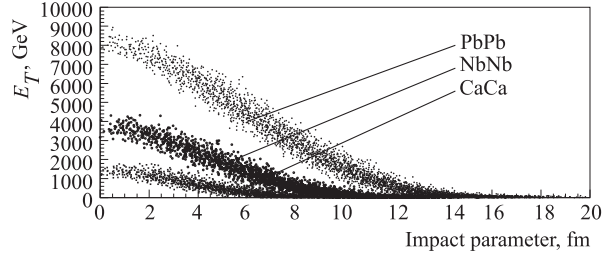


Fig. 2. Correlation between the transverse energy flow E_T in the very forward rapidity $3 \leq |\eta| \leq 5$ and collision impact parameter b . From top to bottom: Pb–Pb, Nb–Nb, Ca–Ca collisions at $\sqrt{s} = 5.5A$ TeV

dependence of the total transverse energy produced in the pseudorapidity interval $3 \leq |\eta| \leq 5$ on the collision impact parameter is presented in Fig. 2. We can see that the plot for E_T - b correlation is diffuse distributions due to fluctuations in nucleus-nucleus collision dynamics: fluctuations of number of nucleon-nucleon subcollisions at given b and fluctuations of transverse energy flow at each nucleon-nucleon interaction. Note that the correlation curve for the total energy flow is of the same shape. The bulk of the energy produced in the very forward direction run up to 10–100 TeV. This allows one to measure the total energy with high accuracy and to reduce experimental errors for the b estimation.

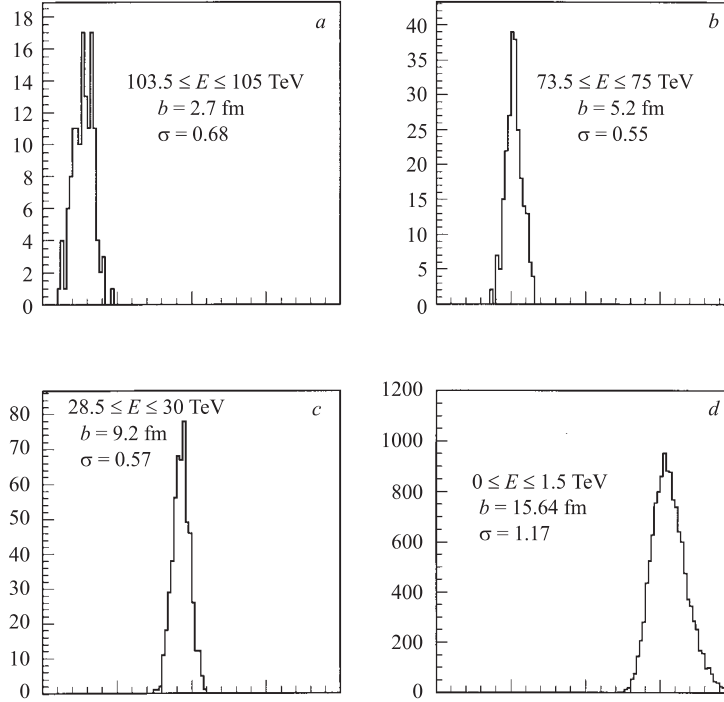


Fig. 3. The Pb–Pb event distributions on the impact parameter at the fixed value of energy deposition in the very forward rapidity region $3 \leq |\eta| \leq 5$

The impact parameter distribution functions at fixing values of the total energy deposition has Gaussian-like form (Fig. 3) with width σ_b dependent on an impact parameter (Fig. 4, *a,b*). We can define the absolute accuracy as $\pm 2\sigma_b$, and for the central collisions ($b \leq 2$ fm) this value lies between 0.2 and 1 fm. For the impact parameter value from 2 up to 12 fm, the accuracy is constant at the ~ 1 fm level and strongly deteriorates up to 2.5 fm for the peripheral collisions ($b \geq 12$ fm). It can be explained by diminution of the energy produced in the explored pseudorapidity region ($3 \leq |\eta| \leq 5$) with a centrality decreasing. At the same time we see that the relative error for the peripheral collisions is minimal (Fig. 4, *a,b*) since in this case the statistics is hardly increased.

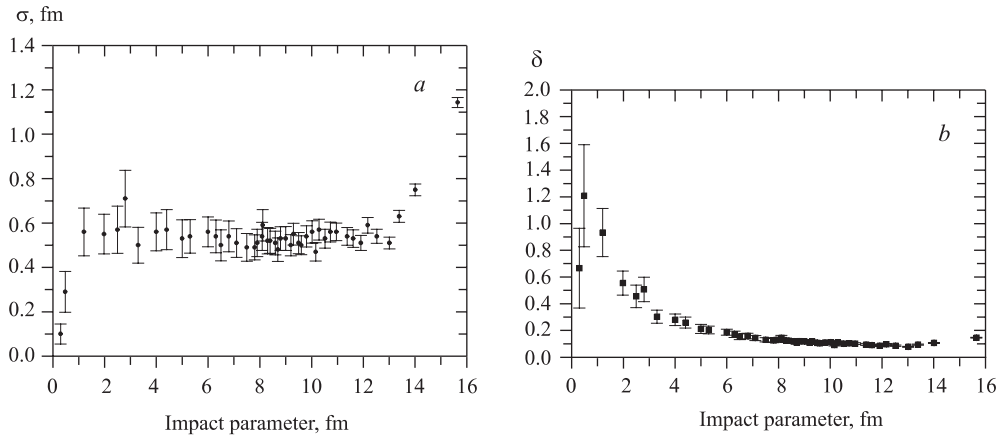


Fig. 4. An impact parameter dependence of the Gaussian width σ_b (a) and the relative error $\delta = 2\sigma_b/b$ (b) for Pb–Pb collisions

We should remark that uncertainties are associated with the use of various parton shadowing models and the sets of structure functions can lead to an ambiguity in E_T - b correlation. In more detail the influence of these aspects on the total (transverse) energy flows is discussed in Ref. [20].

2. POSSIBILITY FOR FAST INELASTIC EVENT SELECTION AND MONITORING

The fast selection of inelastic nucleus-nucleus collisions is one of the basic problems of experimentation with colliding heavy ion beams. A measurement of the collision rate is necessary one to calculate absolute cross section values for particular channels of nuclear interactions and to compare spectra obtained in various experiment modes. Besides, a direct identification of such interactions at a first level trigger is very important for an event-by-event analysis to reach samples of most central events. Moreover, an inelastic interaction trigger allows one to suppress various background processes such as beam collisions with residual gas nuclei as well as with set-up material.

As was shown in [21], there is a significant influence of beam particle interactions of electromagnetic nature like electromagnetic dissociation and electron-positron pair production on the collision rate. For instance, in case of lead-lead collision an electromagnetic interaction rate will exceed a nuclear one by a factor of ≈ 50 . An inelastic interaction trigger makes it possible to separate a part of the interaction rate related to nuclear collisions only.

It should be noted that luminosity of the Large Hadron Collider in nucleus-nucleus collision modes will have variation of a few orders of magnitude for various ion species up to 10^8 s^{-1} in the Ca–Ca mode. This luminosity range is affordable for operation of the CMS detector and an inelastic interaction trigger ought to be enough universal to operate up to the highest rate limit.

One of the critical features of a first level trigger is insensitivity to details of nuclear collision dynamics in the central rapidity region. As it was shown above a very forward pseudorapidity range of $3 < |\eta| < 5$ is not sensitive to the final state reinteraction effects such

as medium-induced jet quenching. Thus, detectors in this region provide suitable basis for inelastic event selection. Below we discuss a simple method of an inelastic nucleus-nucleus collision triggering.

The simulation shows that there is a strong correlation between the energy detected in the positive pseudorapidity (HF1) and negative pseudorapidity (HF2) calorimeter arms for nucleus-nucleus interactions (Fig. 5) [22]. In particular, there is not such a correlation in nuclear interactions with a residual gas. Thus, such an effect will be suppressed events as well as detector noise signals.

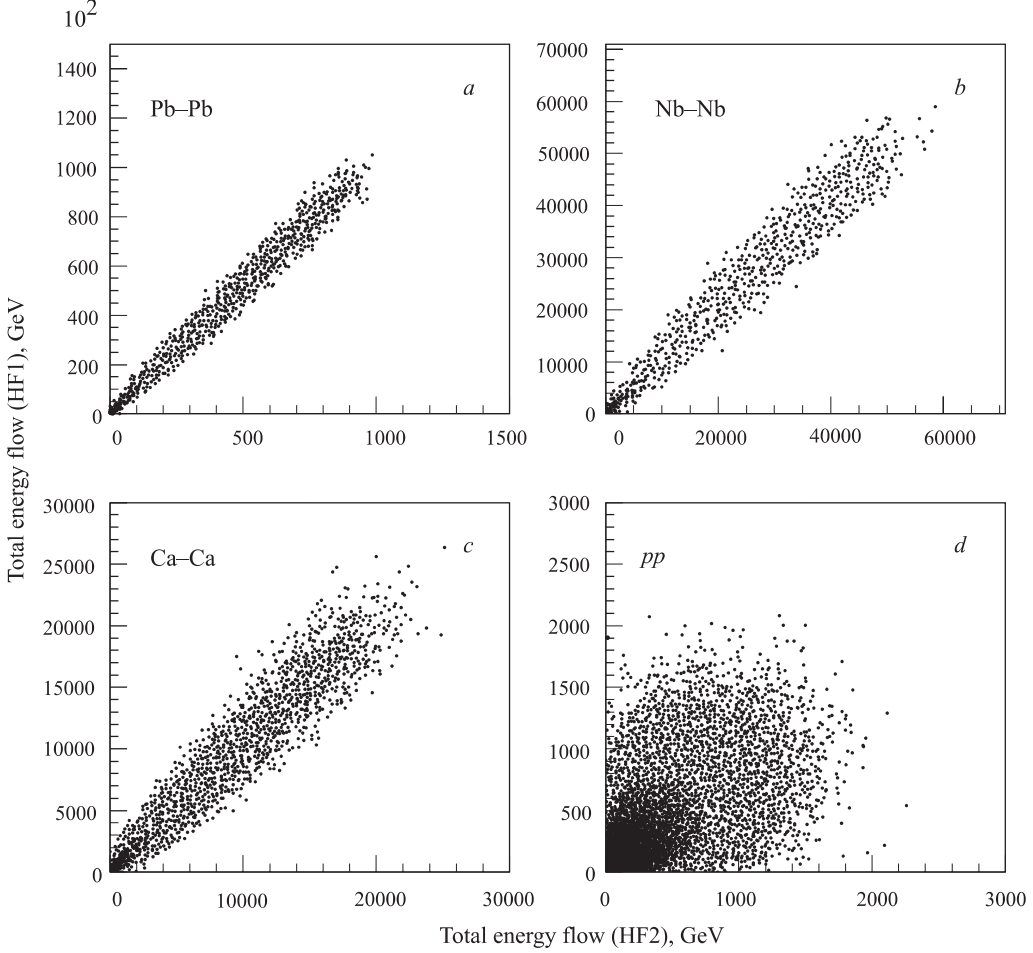


Fig. 5. The correlation plot between total energy flow in pseudorapidity regions $-5 < \eta < -3$ and $3 < \eta < 5$ for Pb-Pb (a), Nb-Nb (b), Ca-Ca (c), pp collisions (d) at $\sqrt{s} = 5.5 A$ TeV

As a basic trigger condition we propose to use a time difference measurement (start-stop) of timing signals from the two very forward calorimeter arms, HF1 and HF2. The event is accepted if the values of the total energy per event, E_{HF1} and E_{HF2} in each of the two

calorimeter arms exceeds a predefined threshold value E_{thr} . Thus, the condition of selection of nucleus-nucleus interactions is defined by the requirement:

$$(E_{\text{HF1}} > E_{\text{thr}})(E_{\text{HF2}} > E_{\text{thr}}).$$

Besides a simple coincidence of a longitudinal coordinate of the interaction vertex might be fixed with precision of about few centimeters in the vicinity of a beam intersection point if the calorimeter provides the time resolution better than 1 ns. The speed of light (30 cm/ns) gives one 30 cm resolution, for the time resolution is equal to 1 ns.

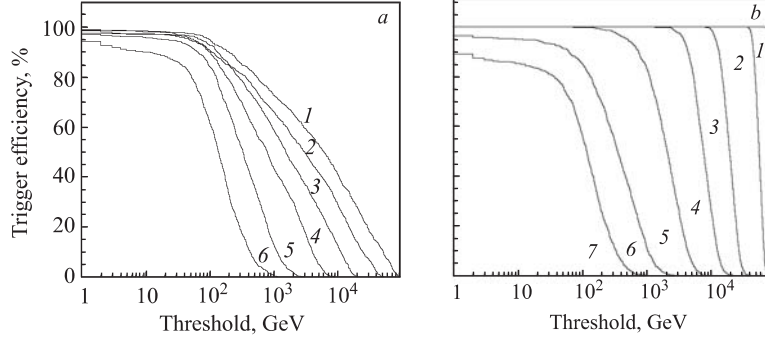


Fig. 6. The efficiency of the event selection: *a*) for minimum bias nucleus-nucleus collisions: 1 — PbPb; 2 — NbNb; 3 — CaCa; 4 — OO; 5 — $\alpha\alpha$; 6 — pp ; *b*) for Pb–Pb collisions at various impact parameter intervals (fm): 1 — 0...2; 2 — 4...6; 3 — 8...10; 4 — 10...12; 5 — 12...14; 6 — 14...16; 7 — 16...18

To justify such solution we have studied a task of an energy threshold dependence of the event selection efficiency, ϵ , defined as

$$\epsilon = N_{\text{trigger}}/N_{\text{simulated}} \cdot 100 \%,$$

where $N_{\text{simulated}}$ is the total number of simulated events, N_{trigger} is the number of events satisfying the selection condition.

Figure 6, *a* shows ϵ behaviour with variation of colliding nucleus mass number. Figure 6, *b* shows efficiency dependence on a collision impact parameter allowing to conclude that with thresholds of 100 GeV in each of arms a Pb–Pb collision selection would not be damaged up to $b < 15$ fm. It might be concluded that event counting stability can be provided at the same threshold value. We note that proton-proton case gives a somewhat lower counting efficiency and introduction of some correction will be necessary in future to obtain unbiased normalization of $dE_T/d\eta$ distributions. We remark also that ϵ does not depend on the nuclear number in the range from Ca up to Pb at the threshold up to 500 GeV. An increase of energy threshold up to 500 GeV leads to an efficiency decreasing only by a few percent for the colliding nuclei with $A \geq 40$. The efficiency drops from 80% down to 30% for the pp collisions.

We believe that being based on a Cherenkov detector technique, the CMS HF calorimeter is able in principle to provide the requested timing measurements, and necessary practical solutions might be foreseen.

3. CMS HF CALORIMETER GEOMETRY AND INSTALLATION

The very forward calorimeters in CMS [5, 23] will cover the pseudorapidity range $3 \leq |\eta| \leq 5$. They improve the missing transverse energy resolution and enable the identification of very forward jets. In all these cases, a moderate calorimeter energy resolution and granularity are needed. A good reconstruction of the energy flow and jet energies demands a degree of equalization of hadron and electromagnetic shower signals. The fast signal speed, narrow

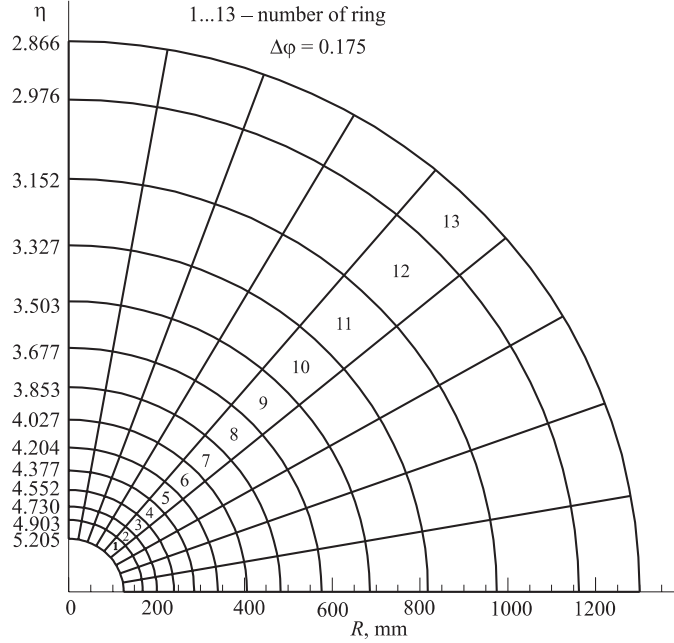


Fig. 7. Hadron Forward Calorimeter: the transverse view

lateral profile and low sensitivity to neutrons and radioactive decays allow for better separation of jets from background with respect to other calorimetric techniques. The noncompensating feature of the quartz fiber calorimeter, however, puts some limitations on the jet energy resolution because the fraction of the energy carried by γ photons strongly fluctuates. The longitudinal segmentation of the calorimeter allows approximate equalization of the signals from γ photons and charged pions of the same energy.

The segmentation of the HF calorimeter is presented in Fig. 7. It contains $26 \times 36 = 936$ towers with $\delta\eta \times \varphi = 0.175 \times 0.175$ granulation. Figure 8 shows the dependence of the reconstructed energy in the ring as a function of η for the γ photons at fixed transverse momentum $p_t = 0.3$ GeV/c (the mean p_t of photons in the minimum bias event) and for negative pions at $p_t = 3$ GeV/c (the mean p_t of pions in the jet). Note that there exist the degradation of the reconstructed energy at $\eta = 4.8$, the reason for which being the screening of this ring from produced particles by the LHC beam pipe in the front of HF calorimeter (see Fig. 9).

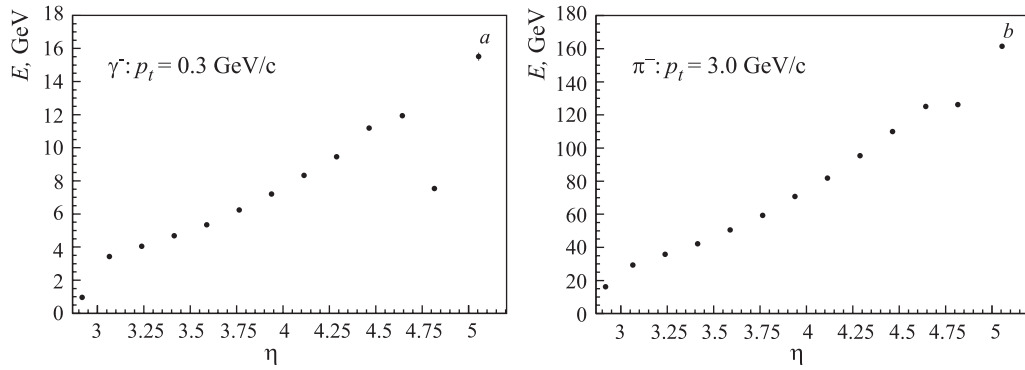


Fig. 8. The reconstructed energy deposition in the ring as the function of η for γ photons with $p_t = 0.3 \text{ GeV/c}$ (a) and π^- with $p_t = 3.0 \text{ GeV/c}$ (b)

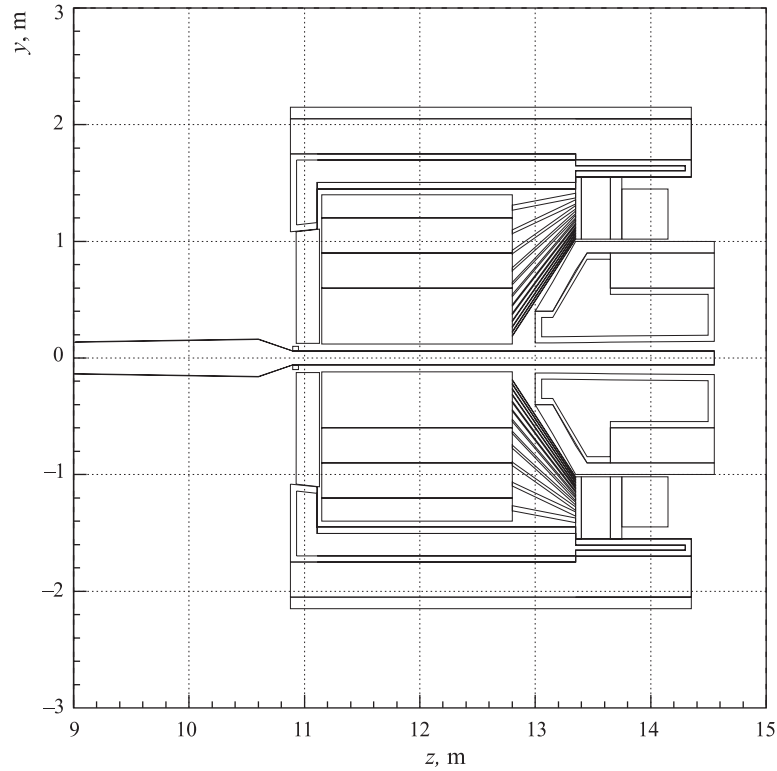


Fig. 9. Beam pipe in the front of HF calorimeter

4. HF CALORIMETER RESPONSE TO ENERGY FLOW

In this section we consider the response of HF CMS calorimetric system to energy flow in heavy ion collisions in more detail.

As in previous sections the HIJING model [14] has been used to generate central Pb–Pb collisions at $\sqrt{s} = 5.5$ A TeV and Ar–Ar collisions at $\sqrt{s} = 6.3$ A TeV. Note that due to insensitivity of very forward rapidity region to final state reinteractions, the corresponding values of mean energy $\langle e \rangle \approx 9.5$ GeV and mean transverse momentum $\langle p_t \rangle \approx 0.35$ GeV of particles are close for Pb–Pb and Ar–Ar collisions of different centrality classes.

HF responses have been obtained by the GEANT-based program package CMSIM 120 (CMS Simulation Package, version 120). One can compare HIJING total energy deposition in the regions of pseudorapidity of the towers of the HF calorimeter and the total responses of the corresponding towers (Fig. 10). We see that the difference between those values is small in the region of pseudorapidity near the centre of HF calorimeters ($|\eta| \sim 4$), but sufficiently large in the beginning and the end of the HF (Fig. 11). For heavy ion collisions HF underestimates about 15 % of the realized energy in the HF pseudorapidity region. The main cause of this effect (the existence of the LHC beam pipe, which screens some region of pseudorapidity) has been demonstrated in the previous section. We can see also from Fig. 10 that the influence of CMS magnetic field $B = 4$ T on total energy flow is not significant for the very forward rapidity region. Let us remark that the influence of the CMS magnetic field is much stronger in the barrel and end-cap parts of CMS calorimetric system, and it results in the visible degradation of transverse energy flow in the CMS central rapidity regions.

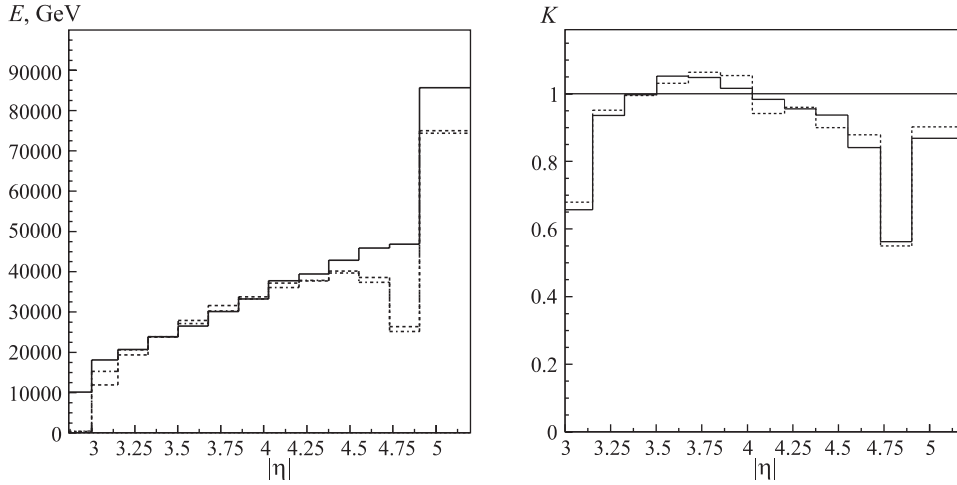


Fig. 10. HIJING total energy $E(\text{hijing})$ in central Pb–Pb collisions (solid histogram) and HF calorimeter response $E(l + s)$ (the sum of energies in towers with long and short fibers) for the cases with (dashed histogram) and without (dash-dotted histogram) CMS magnetic field $B = 4$ T

Fig. 11. Total HF response / HIJING energy deposition ratio for the central Pb–Pb (solid histogram) and Ar–Ar (dashed histogram) collisions, $K = E(l + s)/E(\text{hijing})$

Thus we propose to introduce additional special correction coefficients $1/K(\eta)$ for adequate reconstruction of the total energy flow in the region of pseudorapidity of the HF calorimeter. We have found that these correction coefficients do not show some substantial dependence on centrality (impact parameter) of a collision and are similar for different nuclei (see Fig. 11).

5. IMPACT PARAMETER DETERMINATION WITH HF CALORIMETER

As we have found in Section 2, the very forward pseudorapidity region $3 \leq |\eta| \leq 5$ is almost not sensitive to the final state reinteractions and could potentially provide an adequate measurement of impact parameter via (transverse) energy flow. Since the performance of full GEANT-based simulation of CMS calorimetric system responses on significant number ($\sim 10^3-10^4$) of Pb–Pb events is still not really resolving task due to enormously huge amount of required CPU time and memory, we study the possibility of using HF calorimeter for determination of impact parameter on the example of Ar–Ar collisions. In previous section it was shown that the HF energy flow response pattern is similar for Pb–Pb and Ar–Ar and the same correction procedure should be applied. Thus we can expect the result obtained for Ar–Ar collisions should be at least qualitatively valid also for Pb–Pb case.

We generated 750 Ar–Ar collisions with different impact parameters. In order to reduce our statistical errors for the most central events we add 250 events with impact parameter $b < 4$ fm to 500 minimum bias events.

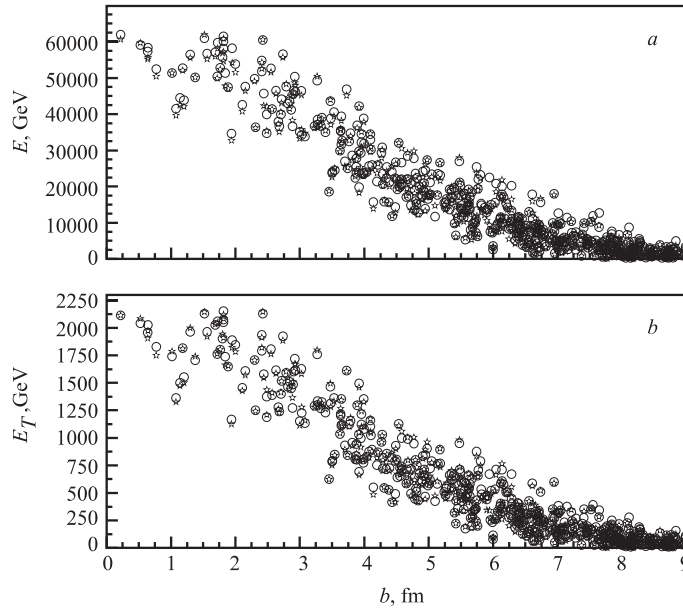


Fig. 12. Correlation between the total (a) and transverse (b) energy deposition in HF and impact parameter of 500 minimum bias Ar–Ar collisions: HIJING predictions (stars) and reconstructed responses (open circles)

Thus the main result of this section is that the finite energy resolution of HF calorimeter does not result in some substantial degradation of accuracy of impact parameter determination in heavy ion collisions.

Figure 12 demonstrates the correlation between the total and transverse energy deposition in HF and impact parameter of 500 minimum bias Ar–Ar collisions. Figure 13 shows the impact parameter dependence of the relative dispersion (normalized Gaussian width) $\sigma_E/\langle E \rangle$ of HF total and transverse energy distribution at fixed b . The value $\sigma_E/\langle E \rangle$ increases with the

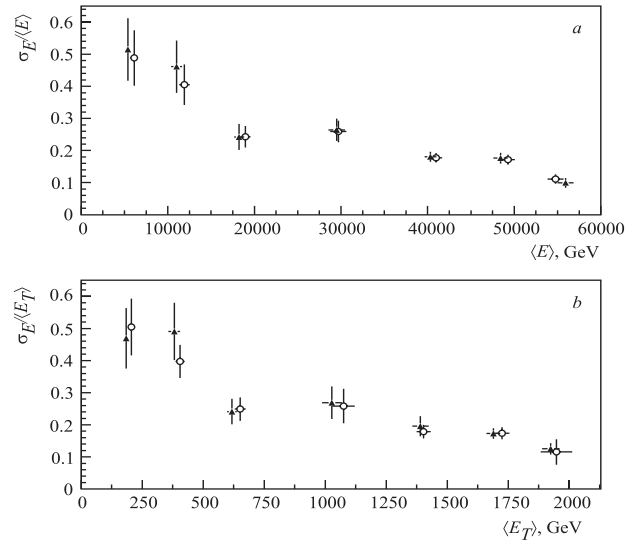


Fig. 13. An impact parameter dependence of the normalized Gaussian width $\sigma_E / \langle E \rangle$ of HF total (a) and transverse (b) energy distribution at fixed b for 750 Ar–Ar collisions: HIJING predictions (triangles) and reconstructed responses (open circles)

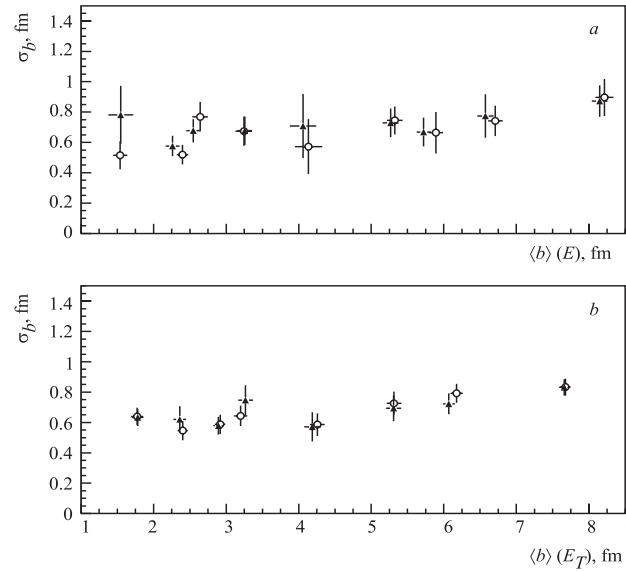


Fig. 14. An impact parameter dependence of the Gaussian width σ_b of b distribution at the fixed value of total (a) and transverse (b) energy deposition in HF for 750 Ar–Ar collisions: HIJING predictions (triangles) and reconstructed responses (open circles)

rise of impact parameter. The values are the same for the realized energy and HF responses within our statistical errors. The behaviour of accuracy of impact parameter determination $2\sigma_b$ (where σ_b is the Gaussian width of impact parameter distribution at the fixed value energy deposition in HF) is close to the result obtained in Section 2 for Pb–Pb collisions: it is approximately constant (within statistical errors) at the $\sim 1\text{--}1.5$ fm level for central and semicentral collisions (Fig. 14) and increases for peripheral collisions up to $\sigma_b \sim 2$ fm for $b > 2R_A \approx 8$ fm. Note that the result is almost the same determining the impact parameter via total energy flow and transverse energy flow for reconstructed responses, as well as for realized HIJING energy.

6. HF CALORIMETER RESPONSE ON FLUCTUATIONS OF HADRONIC-TO-ELECTROMAGNETIC ENERGY RATIO

The structure of HF calorimeter allows one to separate the signal from hadronic (π^\pm, K^\pm, p, n) and electromagnetic ($e^\pm, \pi^0(\rightarrow 2\gamma), \gamma$) component of an event, the latter being determined as a difference between the total energy deposition and the hadronic fraction of it. The one of the challenging tasks at LHC may be searching for exotic events with nonstatistical enhancement of the hadronic-to-electromagnetic energy deposition ratio in an event-by-event analysis, which could be a manifestation of new dynamical effects in the very forward rapidity region, in particular, the quark matter fireball formation (Centauro-like events) [12, 13].

The Monte-Carlo code CNGEN v.1.13 (Centauro Event Generator) has been used to simulate the events with strong fluctuations of hadronic-to-electromagnetic production components [11, 12]. In the framework of this model, the Centauro-fireball is produced near the projectile fragmentation region due to the transformation of kinetic energy of nucleons in a projectile nucleus into heating and formation of a hot quark matter with high baryochemical potential. This results in suppression of density of light antiquarks \bar{u} and \bar{d} due to Pauli blocking. On the other hand, enhancement of strange hadron production is achieved by intensive gluon-gluon fusions, $gg \rightarrow s\bar{s}$. Then the fireball becomes a strange quark matter with relatively long lifetime ($\tau \sim 10^{-13}$ s). Finally, it decays into baryons and light meta-stable strange matter objects with $A > 6$ (the so-called «strangelets»). More than 99% energy of such events goes to hadronic component. The maximum deposition of Centauro energy is predicted to be achieved in the forward rapidity region $4.5 \leq |\eta| \leq 5.5$, partially covered by the CMS HF calorimeter [13].

Figure 15 shows the ratio of responses in short and long fibers of HF calorimeter for «normal» HIJING Pb–Pb events and for Centauro events. Let us mark that the visible enhancement of this ratio at $|\eta| \sim 4.8$ region for HIJING case is due to stronger influence of beam pipe screening on soft γ photons of HIJING as compared to the (semi)hard hadrons of

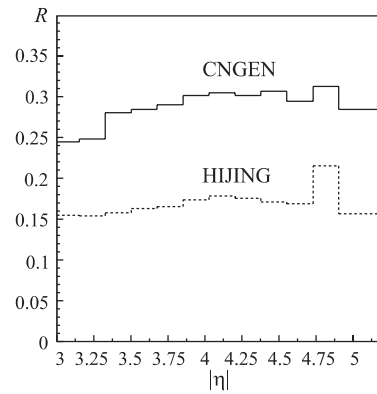


Fig. 15. The «short fiber»-to-«long fiber» energy deposition ratio R in HF towers for Centauro (solid histogram) and HIJING (dashed histogram) central Pb–Pb events

CNGEN (see Fig. 8). The difference of the ratios for two cases by the factor of $\sim 1.5-2$ allows us to believe that the HF calorimeter can be applied for searching exotic events with nonstatistical fluctuations of hadronic-to-electromagnetic energy ratio in an event-by-event analysis.

CONCLUSIONS

To summarize, we have considered the capability of the very forward (HF) calorimeter of CMS detector at LHC to be applied to specific studies with heavy ion beams.

On the basis of the transverse energy calculation performed in the framework of QCD-inspired model we have demonstrated that the transverse energy E_T directly relates with a collision impact parameter b . We have found that the very forward pseudorapidity region $3 \leq |\eta| \leq 5$ is almost insensitive to the final state reinteractions and can provide an adequate measurement of impact parameter via (transverse) energy flow.

Moreover, due to sensitivity of very forward rapidity region to the collision nuclear geometry only, this region can also be used for fast selection of inelastic nucleus-nucleus collisions basing on the strong correlation between the energy flow in positive ($\eta > 0$) and negative ($\eta < 0$) calorimeter arms.

We have found that the total energy flow in very forward rapidity region can be reconstructed by HF calorimeter when the correction coefficients procedure is applied. The influence of CMS magnetic field on the energy reconstruction efficiency is not expected to be significant for HF domain. The finite energy resolution of HF calorimeter is shown to result in no substantial degradation of accuracy of impact parameter determination, which is of the order of 1–1.5 fm for Ar–Ar and Pb–Pb collisions up to $b \sim 2R_A$ and gets worse by the factor of ~ 2 for very peripheral ($b > 2R_A$) events.

We also suggest to apply the very forward CMS calorimeter to the search for exotic events with nonstatistical fluctuations of hadronic-to-electromagnetic energy ratio, which could be a signal of new dynamical effects like quark matter fireball formation.

Finally, the Monte Carlo study shows that the very forward CMS HF calorimeter is well suited for the investigation of the number of various aspects of heavy ion collisions: impact parameter determination, fluctuations of hadronic-to-electromagnetic energy ratio, fast inelastic event selection.

Acknowledgments. It is a pleasure to thank M. Bedjidian, D. Denegri, V.B. Gavrilo and I.A. Golutvin for encouraging and interest to the work. Discussions with A.I. Zarubin, A.I. Demianov, A.M. Gribushin, M.V. Savina, N.V. Slavin, A.M. Snigirev and A.A. Yershov are gratefully acknowledged. We would like to thank S.A. Sadovsky for providing the program CNGEN.

REFERENCES

1. *Harris J.W., Müller B.* // Ann. Rev. Nucl. Part. Sci. 1996. V.46. P.71.
2. *Lokhtin I.P., Sarycheva L.I., Snigirev A.M.* // Phys. Part. Nucl. 1999. V.30. P.279.
3. *Bass S.A. et al.* // J. Phys. G. 1999. V.25. P.R1.
4. ALICE Collaboration Technical Proposal. CERN/LHCC 95-71. 1995.
5. CMS Collaboration Technical Proposal. CERN/LHCC 94-38. 1994.

6. *Bedjidian M. et al.* Heavy Ion Physics Programme in CMS. CERN CMS Note 2000/060.
7. *Lokhtin I.P., Snigirev A.M.* High-Mass Dimuon and Secondary J/ψ Production at CMS as Probes of Medium-Induced Bottom Quark Energy Loss in Heavy Ion Collisions. CERN CMS Note 2001/008.
8. *Eskola K.J., Kajantie K., Ruuskanen P.V.* // Phys. Lett. B. 1994. V.332. P.191; Eur. Phys. J. C. 1998. V.1. P.627;
Eskola K.J. // Prog. Theor. Phys. Suppl. 1997. V.129. P.1; Comments Nucl. Part. Phys. 1998. V.22. P.185;
Eskola K.J., Tuominen K. // Phys. Lett. B. 2000. V.489. P.329;
Eskola K.J. et al. // Nucl. Phys. B. 2000. V.570. P.379.
9. *Bjorken J.D.* // Int. J. Mod. Phys. A. 1992. V.7. P.4189;
Donnachie A., Landshoff P. // Nucl. Phys. B. 1988. V.303. P.634.
10. *Savina M.V. et al.* // Phys. At. Nucl. 1999. V.62. P.2084; JINR Rapid Commun. 1998. No.1[87]. P.45; JINR Rapid Commun. 1998. No.5[91]. P.65.
11. *Panagiotou A.D., Karabarounis A., Petridis A.* // Z. Phys. A. 1989. V.333. P.355.
12. *Gladysz-Dziadus E. et al.* Simulation of Centauro Events at CASTOR. CERN ALICE Internal Note 1997/06;
Gladysz-Dziadus E., Panagiotou A.D. Particles from Centauro Decay in the CASTOR Detecting System. CERN ALICE Internal Note 1997/16.
13. *Lokhtin I.P., Petrushanko S.V., Sarycheva L.I.* Preprint of SINP MSU, 1999-33/591.
14. *Gyulassy M., Wang X.-N.* // Phys. Rev. D. 1991. V.44. P.3501; Comp. Phys. Commun. 1994. V.83. P.307.
15. *Arneodo M. et al. (EM Collaboration)* // Nucl. Phys. B. 1997. V.483. P.3; Nucl. Phys. B. 1995. V.441. P.12; Nucl. Phys. B. 1990. V.333. P.1;
Amaudruz B. et al. (NM Collaboration) // Z. Phys. C. 1991. V.51. P.387;
Adams M.R. et al. (E665 Collaboration) // Phys. Rev. Lett. 1992. V.68. P.3266; Phys. Lett. B. 1992. V.287. P.375.
16. *Andersson B. et al.* // Nucl. Phys. B. 1987. V.281. P.289.
17. *Nilson-Almqvist B., Stenlund E.* // Comp. Phys. Commun. 1987. V.43. P.387.
18. *Wang X.N.* // Phys. Rep. 1997. V.280. P.287.
19. *Baier R., Schiff D., Zakharov B.G.* // Annual Rev. Nucl. Part. Sci. 2000. V.50. P.37.
20. *Zarubin P.I., Savina M.V., Shmatov S.V.* JINR Preprint P2-2000-112. Dubna, 2000; Phys. At. Nucl. (in press).
21. *Brandt D., Eggert K., Morsch A.* CERN AT/94-05(DI), SL/94-04(AP), LHC Note 1994/264.
22. *Krasnov V.A. et al.* // JINR Rapid Commun. 1998. No.1[87]. P.39.
23. CMS Collaboration Technical Design Report «The Hadron Calorimeter Project». CERN/LHCC 97-31. 1997.

Received on July 12, 2001.